ARTICLE

Exploring the Low-Temperature Oxidation Chemistry of Cyclohexane in a Jet-Stirred Reactor: an Experimental and Kinetic Modeling Study[†]

Jia-biao Zou[a], Wei Li[a], Li-li Ye[a], Xiao-yuan Zhang[a,b], Yu-yang Li[a,b*], Jiu-zhong Yang[c], Fei Qi[a,b*]

a. Key Laboratory for Power Machinery and Engineering of MOE, Shanghai Jiao Tong University, Shanghai 200240, China
b. Collaborative Innovation Center for Advanced Ship and Deep-Sea Exploration (CISSE), Shanghai 200240, China
c. National Synchrotron Radiation Laboratory, University of Science and Technology of China, Hefei 230029, China

(Dated: Received on June 7, 2018; Accepted on July 3, 2018)

We report the investigation on the low-temperature oxidation of cyclohexane in a jet-stirred reactor over 500−742 K. Synchrotron vacuum ultraviolet photoionization mass spectrometry (SVUV-PIMS) was used for identifying and quantifying the oxidation species. Major products, cyclic olefins, and oxygenated products including reactive hydroperoxides and high oxygen compounds were detected. Compared with *n*-alkanes, a narrow low-temperature window (∼80 K) was observed in the low-temperature oxidation of cyclohexane. Besides, a kinetic model for cyclohexane oxidation was developed based on the CNRS model [Combust. Flame **160**, 2319 (2013)], which can better capture the experimental results than previous models. Based on the modeling analysis, the 1,5-H shift dominates the crucial isomerization steps of the first and second O_2 addition products in the low-temperature chain branching process of cyclohexane. The negative temperature coefficient behavior of cyclohexane oxidation results from the reduced chain branching due to the competition from chain inhibition and propagation reactions, *i.e.* the reaction between cyclohexyl radical and O_2 and the decomposition of cyclohexylperoxy radical, both producing cyclohexene and HO_2 radical, as well as the decomposition of cyclohexylhydroperoxy radical producing hex-5-en-1-al and OH radical.

Key words: Cyclohexane, Low-temperature oxidation, Synchrotron vacuum ultraviolet photoionization mass spectrometry, Kinetic model, Negative temperature coefficient behavior

I. INTRODUCTION

Low-temperature combustion techniques for internal combustion engines have attracted great attentions due to the features to reduce emissions, leading to a growing need to understand low-temperature oxidation chemistry of transportation fuels and their components [1–3]. In particular, the negative temperature coefficient (NTC) behavior typically happening at 500−900 K plays a key role in low-temperature autoignition processes [4, 5]. Naphthenes (cycloalkanes and alkylcycloalkanes) are an important component family in petroleum-derived transportation fuels. Their total volume fraction can reach up to 35% in diesel oils, 20% in jet fuels, and 10% in gasoline [6, 7], while the value can be 50%−70% in diesel oils derived from oil-sands [8]. NTC behavior has also been found in low-temperature oxidation of naphthenes. However, chemistry in naphthene oxidation, especially for the NTC behavior, was still not well understood compared with those in acyclic alkane oxidation. Cyclohexane is one of the smallest naphthenic components in transportation fuels and serves as a model compound for large naphthenic components in transportation surrogate fuels [9, 10]. Further understanding of the low-temperature oxidation chemistry of cyclohexane will not only contribute to the development of accurate kinetic models for transportation surrogate fuels, but also help understand the low-temperature oxidation chemistry of naphthenes.

Various studies have been conducted for the high-temperature combustion of cyclohexane, such as measurements of ignition delay time in shock tubes (ST) [11–15], laminar flame speed in spherical expanding flames [16–18] and counterflow flames [19, 20], and species concentration in flames [16, 21–23], jet-stirred reactor (JSR) oxidation [24, 25] and flow reactor pyrolysis [26]. Compared to the high-temperature combustion of cyclohexane, there are only a limited number of

[†]Part of the special issue for celebration of "the 60th Anniversary of University of Science and Technology of China and the 30th Anniversary of Chinese Journal of Chemical Physics".

*Authors to whom correspondence should be addressed.
E-mail: yuygli@sjtu.edu.cn, fqi@sjtu.edu.cn

studies conducted on its low-temperature oxidation. Lemaire *et al.* [27] measured the ignition delay time of cyclohexane at 600−900 K and 7−14 bar in a rapid compression machine (RCM) and found that the low-temperature oxidation of cyclohexane shows slight NTC behavior. Recently, Vranckx *et al.* [28] extended the pressure up to 40 bar and clearly confirmed the NTC behavior of cyclohexane oxidation between 680−910 K at various pressures and equivalence ratios. Serinyel *et al.* [18] used gas chromatography (GC) to detect stable species in the JSR oxidation of cyclohexane, including cyclic ethers, ketones, aldehydes, and some cyclic olefins. They also found that cyclohexane only has weak reactivity in low-temperature oxidation. Yang *et al.* [29] elucidated this weak reactivity is because the six-membered ring structure limits the number of hydrogen atoms available to the 1,5-H shift, based on their observations in motored-engine experiments and conformational analysis. However, there is no measurement on reactive intermediates in low-temperature oxidation of cyclohexane, such as hydroperoxides and high oxygen compounds (*i.e.* $C_6H_{10}O_3$ species in this work), which play crucial roles in the low-temperature chain branching process.

Buda *et al.* [30] developed a kinetic model for low-temperature oxidation of cyclohexane with estimated rate constants by analog with alkanes. Later, rate constants for the isomerization reactions of the cyclohexylperoxy radical (ROO) and the decomposition reactions of cyclohexylhydroperoxy radicals (QOOH) were updated according to the theoretical work of Sirjean *et al.* [31, 32]. Recently, some rate constants for the formation and decomposition of key oxygenated species were updated by Serinyel *et al.* [18] based on the validation against their JSR oxidation and laminar flame speed data, while they also added some new reactions with the rate constants estimated using the EXGAS software. The final model reported by Serinyel *et al.* [18] shows reasonable agreement with the detailed species concentration data in JSR oxidation over 500−1100 K, as well as the ignition delay time data over 650−1150 K [11–13, 27, 28] and the laminar flame speed data [17–20]. However, its performance in predicting the reactive hydroperoxides and high oxygen compounds, is still unknown due to the absence of experimental measurements.

In this work, the low-temperature oxidation of cyclohexane was investigated in a jet-stirred reactor at atmospheric pressure. Oxidation species were detected using synchrotron vacuum ultraviolet photoionization mass spectrometry (SVUV-PIMS), while their mole fractions were evaluated. The energy barriers of the isomerization pathways in second O_2 addition processes were calculated to reveal the dominant pathway. A kinetic model of cyclohexane oxidation was developed from the model of Serinyel *et al.* (referred to as the Serinyel model) [18] and validated against the present experimental data. Both rate of production (ROP) and sensitivity analysis were performed to provide insight into the low-temperature oxidation chemistry of cyclohexane.

II. EXPERIMENTS

The experiment was performed at the National Synchrotron Radiation Laboratory (NSRL) in Hefei, China. The VUV beamline and the JSR oxidation apparatus were introduced in our recent work [33–35], only brief introduction about the JSR oxidation apparatus will be provided here. An electrically heated silica JSR with a volume of 102 cm^3 was used in this work. The reactor temperature was monitored by a K-type thermocouple mounted in the center of the reactor. Cyclohexane was fed by a liquid chromatography pump and vaporized in an electrically heated vaporizer before mixing with O_2 and Ar. The inlet mole fractions of cyclohexane and O_2 were maintained at 1% and 9%, respectively, corresponding to the stoichiometric condition. The mixture first entered an annular preheating zone which was heated to the reaction temperature in order to minimize thermal gradients in the gas phase inside the reactor [36]. The residence time of gas mixture inside the annular preheater is very short compared to its residence time inside the reactor (a few percent). The experiment was performed at 760 Torr and 500−742 K with the residence time of 2 s. The products were sampled by a quartz nozzle mounted on the sidewall of the reactor. After ionized by the synchrotron VUV light, the ions were detected by a homemade time-of-flight mass spectrometer with a mass resolution ($m/\Delta m$) of 2100 [33].

The mole fractions of products were evaluated using the method introduced elsewhere [37]. Photoionization cross sections (PICSs) of most species were taken from our online database [38]. For hydroperoxides, the PICSs were estimated using the group addition method [39]. The uncertainties of evaluated mole fractions are about ±20% for major species, ±50% for intermediates with known PICSs, and a factor of 2 for those with estimated PICSs [34].

III. KINETIC MODELING

In this work, the sub-mechanism of cyclohexane was updated according to the validation against the present experimental data. Detailed information about the reactions and the source of updated rate constants are listed in Table I, while some controversial reactions will be discussed in this section.

Isomerization of cyclohexylperoxy radical via intramolecular hydrogen transfer mainly produces three cyclohexylhydroperoxy radicals, *i.e.* βQOOH (R2), γQOOH (R3), δQOOH (R4), while the formation of αQOOH through a four-membered ring transition state is not preferred. The rate constants of these isomerization reactions were estimated in most of previous mod-

DOI:10.1063/1674-0068/31/cjcp1806135

TABLE I The reactions updated in the present model[a].

Reaction	A	n	E_a/(cal/mol)	Reference	No.
Isomerization					
$C_6H_{11}OO=\alpha QOOH$[b]	5.25×10^{8}	1.355	38850	PM[c]	R1
$C_6H_{11}OO=\beta QOOH$	5.25×10^{6}	1.739	30250	PM	R2
$C_6H_{11}OO=\gamma QOOH$	1.82×10^{8}	1.401	31740	PM	R3
$C_6H_{11}OO=\delta QOOH$	8.70×10^{7}	1	25556	PM	R4
Chain termination					
$C_6H_{11}+O_2=C_6H_{10}\#6+HO_2$	3.90×10^{12}	0	5000	[30]	R5
$C_6H_{11}OO=C_6H_{10}\#6+HO_2$	7.60×10^{12}	0	32100	[40]	R6
$O_2+\gamma QOOH=C_6H_9OOH\text{-}1+HO_2$	5.20×10^{12}	0	5000	This work	R7
$O_2+\gamma QOOH=C_6H_9OOH\text{-}2+HO_2$	5.20×10^{12}	0	5000	This work	R8
Formation of hex-5-en-1-al and $C_6H_{10}O_3$ and decomposition of $C_6H_{10}O_3$					
$\gamma QOOH\rightarrow OH+$hex-5-en-1-al	9.90×10^{12}	0.248	20440	PM	R9
$OO\gamma QOOH\rightarrow OH+C_6H_{10}O_3$	1.80×10^{7}	1.668	25100	[18]	R10
$C_6H_{10}O_3\rightarrow OH+C_2H_4+CH_2CO+CH_2CHO$	1.50×10^{15}	0	32000	[40, 41]	R11
H-atom abstraction					
$C_6H_{12}+OH=C_6H_{11}+H_2O$	7.70×10^{7}	2	−770	[30]	R12

[a] The rate constants ($k=AT^n\exp(-E_a/RT)$, $cm^3mol^{-1}s^{-1}$) are valued at 1 atm.
[b] βQOOH, γQOOH, and δQOOH: Radical sites are in the ortho, meta, and para positions of the OOH sidechain, respectively.
[c] PM denotes evaluated rate constant in the present model.

els [30, 42, 45, 46]. Cavallotti *et al.* [40] and Sirjean *et al.* [32] calculated the rate constants of the isomerization reactions of ROO and the decomposition reactions of QOOH producing cyclic ethers with modified G2MP2 and CBS-QB3 methods, respectively. Fernandes *et al.* [44] determined the rate constant of R3 using pulsed-laser photolytic initiation combined with laser-induced fluorescence measurements. The rate constants of R2−R4 in the present model and from literature are compared in FIG. 1. Recognizing the great discrepancies of their rate constants among different sources, the rate constants of R2−R4 were evaluated in this work based on the validation against the present experimental data, which mainly locate inside the distributions of literature rate constants. As shown in FIG. 1, the rate constant of R3 is more than one order of magnitude higher than R2 and R4, implying its critical role in determining the low-temperature oxidation reactivity of cyclohexane. Thus, the decomposition of γQOOH will also play an important role in the low-temperature oxidation of cyclohexane. The rate constants in previous models [18, 43] and from theoretical calculations [32, 40] of R9 (a global reaction from γQOOH to hex-5-en-1-al and OH radical) are plotted in FIG. 1(d). The evaluated rate constant in the present model is embedded in the two computed results [31, 40], and is slightly higher than that in the Serinyel model [18].

The formation of cyclic olefins and less reactive HO_2 radical was considered as the chain-inhibition step in low-temperature oxidation since the HO_2 radical favors self-combination reaction to yield H_2O_2 which is thermally stable below 800 K. In the present model, the rate constant recommended by Buda *et al.* [30] was adopted for R5. For R6, the rate constant was taken from the theoretical calculation work of Cavallotti *et al.* [40], while the rate constants of R7 and R8 were estimated in the present model.

For the decomposition of $OO\gamma QOOH$ and high oxygen compounds (lumped as $C_6H_{10}O_3$ in both the Serinyel model and the present model), global reactions were incorporated, which is similar to the previous models [18, 41, 47]. Their rate constants were assigned according to the validation against present experiment. For example, the rate constant of $C_6H_{10}O_3$ decomposition reaction (R11) was evaluated to match the present experiment data according to the rate rule summarized by Ranzi *et al.* [41].

The final model is composed of 437 species and 2376 reactions. The simulation work was performed using the perfectly stirred reactor (PSR) module in the Chemkin-Pro software [48]. Fix gas temperature and transient solver were used. The surface temperature is selected to be the same as the gaseous temperature.

IV. RESULTS AND DISCUSSION

A. Measurement of oxidation species

Benefitting from the use of SVUV-PIMS diagnostic method, detailed speciation, especially for those reactive intermediates, was achieved in this work. As shown

DOI:10.1063/1674-0068/31/cjcp1806135

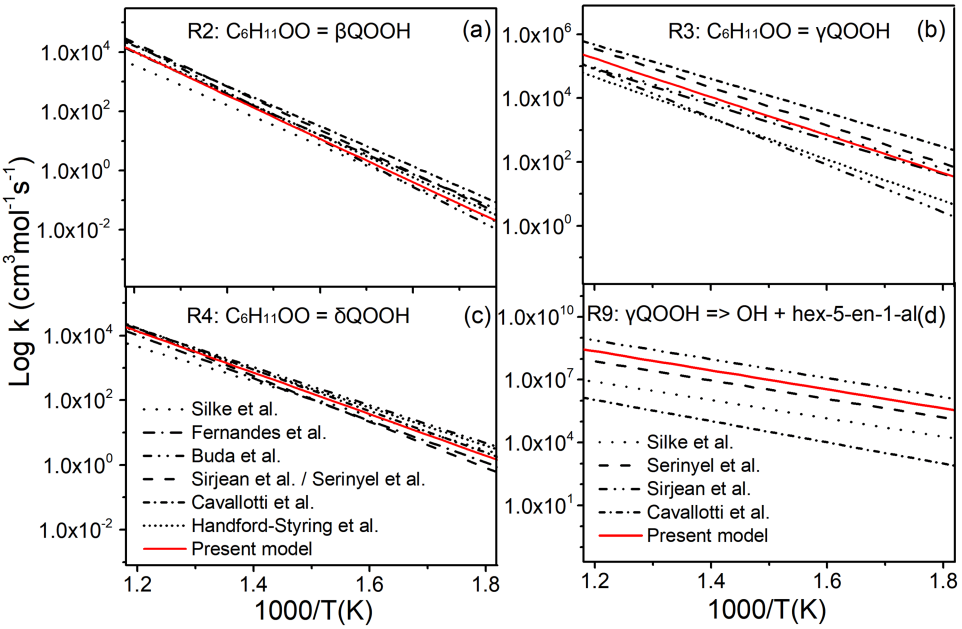

FIG. 1 (a)−(c) Comparison between the rate constants of R2, R3, and R4 in the present model and from Refs.[18, 30, 32, 40, 42–44]; (d) Comparison between the rate constants of R9 in the present model and from Refs.[18, 31, 40, 43].

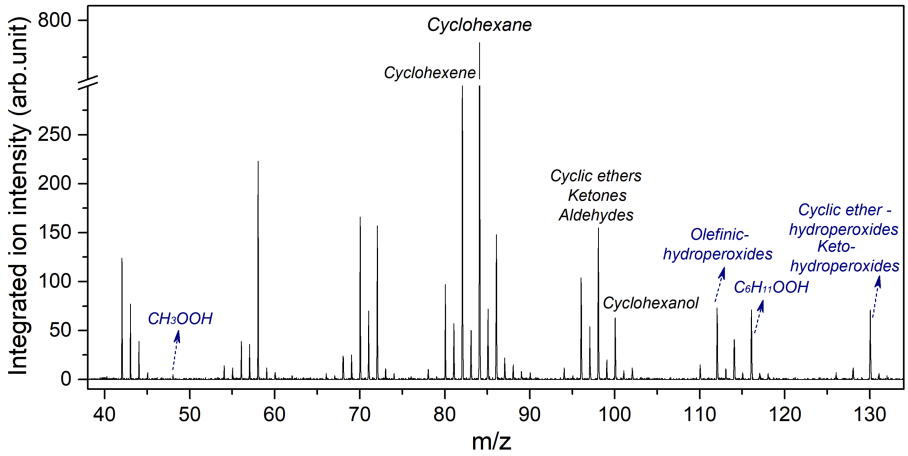

FIG. 2 Mass spectrum of cyclohexane oxidation at 600 K, equivalence ratio ϕ=1.0 and the photon energy of 10.00 eV. The formula and names in blue color denote hydroperoxides observed in this work.

in FIG. 2, stable oxidation products were measured in this work, including cyclic ethers/aldehydes/ketones, cyclic olefins and cyclic alcohols, which were also observed by Serinyel *et al.* [18]. However, the GC method used in the work of Serinyel *et al.* [18] is not capable to detect reactive intermediates like hydroperoxides. In this work, hydroperoxides including methyl hydroperoxide (CH_3OOH), cyclohexyl hydroperoxide ($C_6H_{11}OOH$), cyclic ether hydroperoxides (CEHPs), keto-hydroperoxides (KHPs) and olefinic-hyderperoxides (OFHPs), as well as their decomposition products, were successfully detected. Particularly, the signal at m/z=130.05 ($C_6H_{10}O_3$) is referred to KHPs/CEHPs which are critical chain-branching trigers [49].

B. Consumption of cyclohexane

FIGs. 3−5 shows the measured mole fraction profiles of reactants, major products, and intermediates. As a comparison, the predicted results by the present model, the Serinyel model [18] and the model of Silke *et al.* (referred to as the Silke model) [11] are also shown in FIG. 3. As shown in FIG. 3, the measured mole fraction profile of cyclohexane shows a low-temperature window of about 80 K, which is composed by a low-temperature

DOI:10.1063/1674-0068/31/cjcp1806135

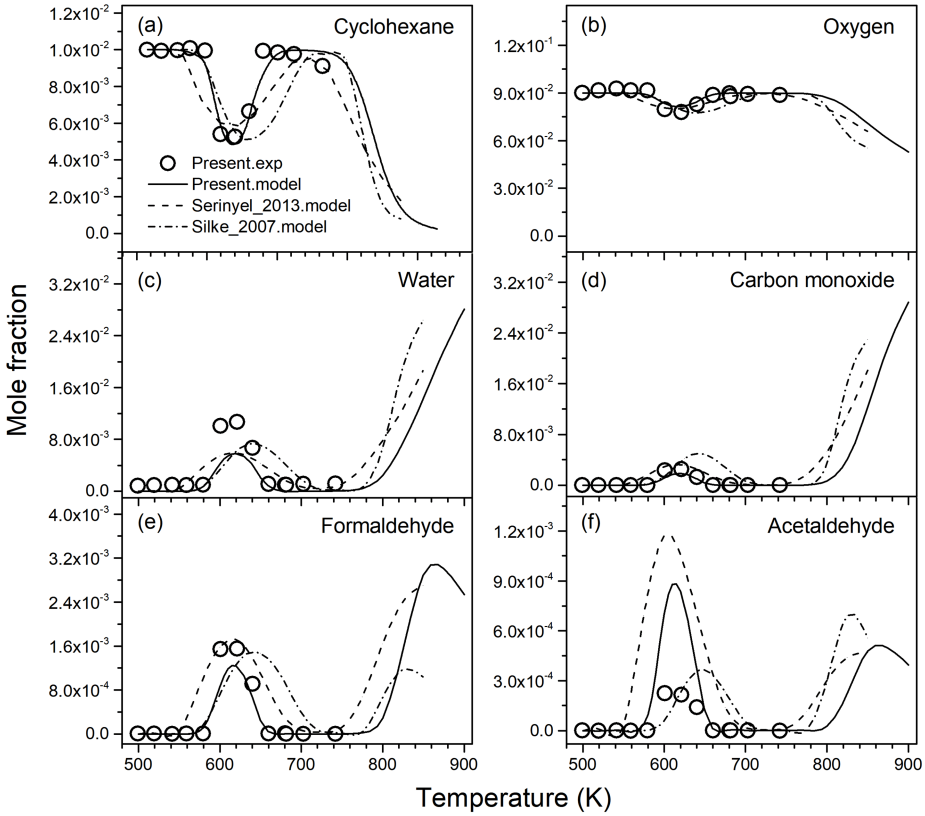

FIG. 3 Measured (symbols) and predicted (lines) mole fraction profiles of major species in the oxidation of cyclohexane. Solid, dash, and dash dot lines represent the predicted results by the present model, the Serinyel model [18], and the Silke model [43], respectively.

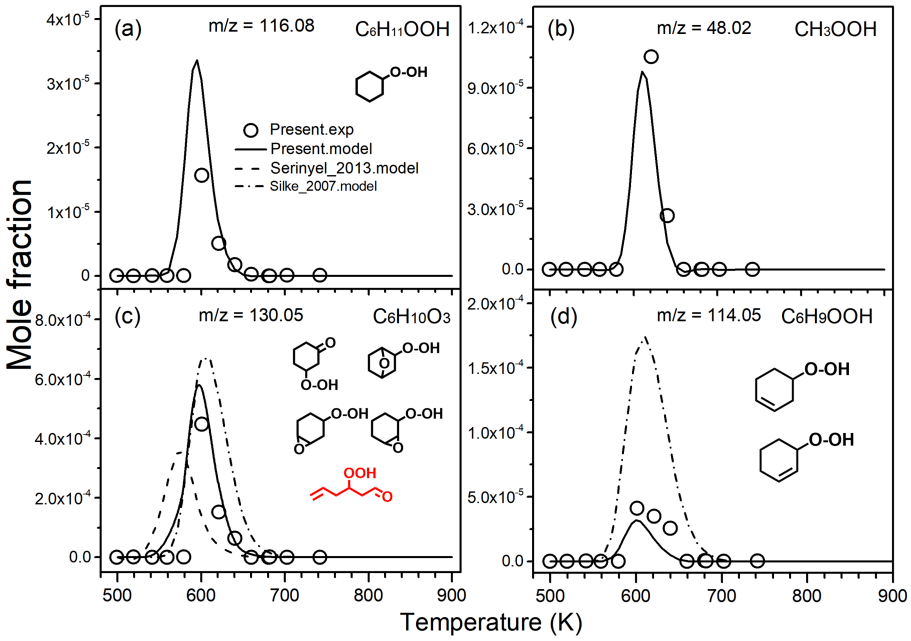

FIG. 4 Measured (symbols) and predicted (lines) mole fraction profiles of hydroperoxides and high oxygen compounds. Solid, dash, and dash dot lines represent the predicted results by the present model, the Serinyel model [18], and the Silke model [43], respectively.

DOI:10.1063/1674-0068/31/cjcp1806135

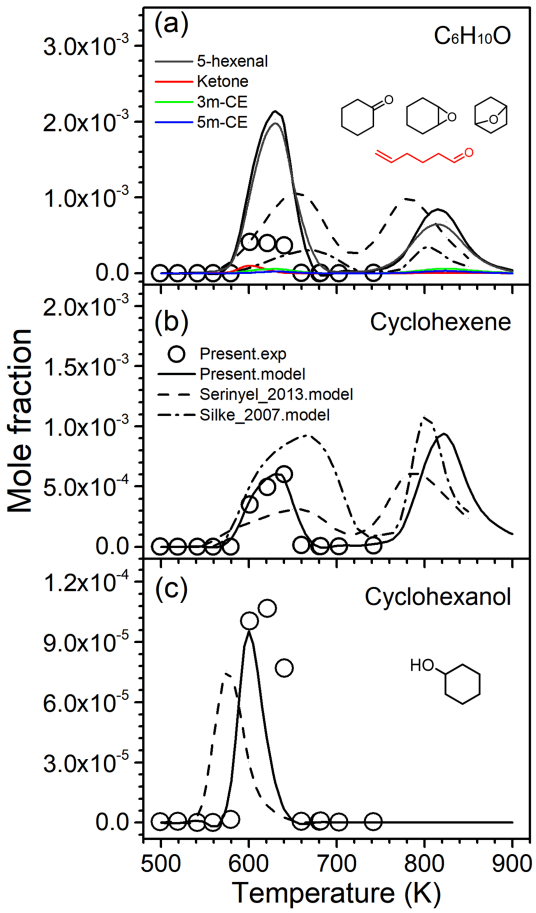

FIG. 5 Measured (symbols) and predicted (lines) mole fraction profiles of intermediates produced from the first O_2 addition process. Solid, dash, and dash dot lines represent the predicted results by the present model, the Serinyel model [18], and the Silke model [43], respectively. 3m-CE and 5m-CE represent three- and five-membered cyclic ether, respectively.

oxidation region (first half, 580−620 K) and a NTC region (second half, 620−660 K). The low-temperature window is much narrower than its acyclic counterparts, *e.g.* *n*-hexane (about 200 K) [50]. Under the conditions investigated by Serinyel *et al.* [18], the measured low-temperature window of cyclohexane oxidation was even narrower (about 55 K). The measured mole fraction profiles of major products also indicate a similar narrow temperature window. As shown in FIG. 3, the present model can well capture the measured low-temperature window, while the two previous models both over-predict the temperature window.

In order to explore the low-temperature oxidation chemistry of cyclohexane, both the ROP analysis and the sensitivity analysis were conducted at 575 and 660 K, corresponding to the low-temperature oxidation region and the NTC region, respectively. Based on the ROP analysis, the reaction networks at 575 and 660 K are drawn in FIG. 6 to guide the eye. The sensitivity analysis for the consumption of cyclohexane is shown in FIG. 7. As concluded by Battin-Leclerc *et al.* [51] and Zádor *et al.* [52], cyclohexane has a similar low-temperature reaction mechanism to its acyclic counterparts. Cyclohexane is mainly consumed via the H-atom abstraction reaction by OH radical (R12) (97.2% and 95.4% at 575 and 660 K, respectively). It is worth noting that, the ROP analysis at 575 K demonstrates R9, R10, and R11 produce more than 60% of OH radical. As temperature increases, the H-atom abstraction reaction by HO_2 has an increasing contribution (0.5% and 3.8% at 575 and 660 K, respectively). In the low-temperature oxidation of alkanes, the low-temperature oxidation reactivity is determined by the competition between chain branching and chain inhibition/termination, which results in the NTC behavior [51]. Thus, the following discussion will be focused on this competition in the chain reaction system of low-temperature oxidation of cyclohexane.

C. Low-temperature chain branching process and NTC behavior

According to the ROP analysis and the sensitivity analysis, the chain branching process (see Scheme 1), including (1) the first O_2 addition to R (cyclohexyl radical) forming ROO (cyclohexylperoxy radical), (2) the isomerization of ROO to QOOH (cyclohexylhydroperoxy radical) through intramolecular H shift (R3), (3) the second O_2 addition to QOOH forming OOQOOH, (4) the isomerization of OOQOOH to $U(OOH)_2$, (5) the decomposition of $U(OOH)_2$ forming ketohydroperoxide and OH radical, and (6) the sequential decomposition of ketohydroperoxide forming the second OH radical (R11), plays a crucial role in the low-temperature oxidation of cyclohexane, which is similar to the situation in the low-temperature oxidation of alkanes [49, 51]. In both the Serinyel model [18] and the present model, steps (4) and (5) were lumped as one global reaction (R10). In particular, most steps in the chain branching process are among the most sensitive reactions for promoting the consumption of cyclohexane at both 575 and 660 K, as shown in FIG. 7.

The first O_2 addition reaction consumes most of cyclohexyl radical, making it the dominant consumption pathway of cyclohexyl radical in low-temperature oxidation. Furthermore, the reaction of cyclohexyl radical with O_2 producing cyclohexene and HO_2 (R5), which is the step (7) in Scheme 1, plays a minor role in the consumption of cyclohexyl radical. As the temperature increases from 575 K to 660 K, this reaction shows enhanced competition to the first O_2 addition reaction, with the contribution increasing from 5.0% at 575 K to 10.9% at 660 K. It should be noted that this reaction is a typical chain inhibition reaction since it produces HO_2 radical which is much less reactive than H atom, O atom, and OH radical. As a result, the sensitiv-

DOI:10.1063/1674-0068/31/cjcp1806135

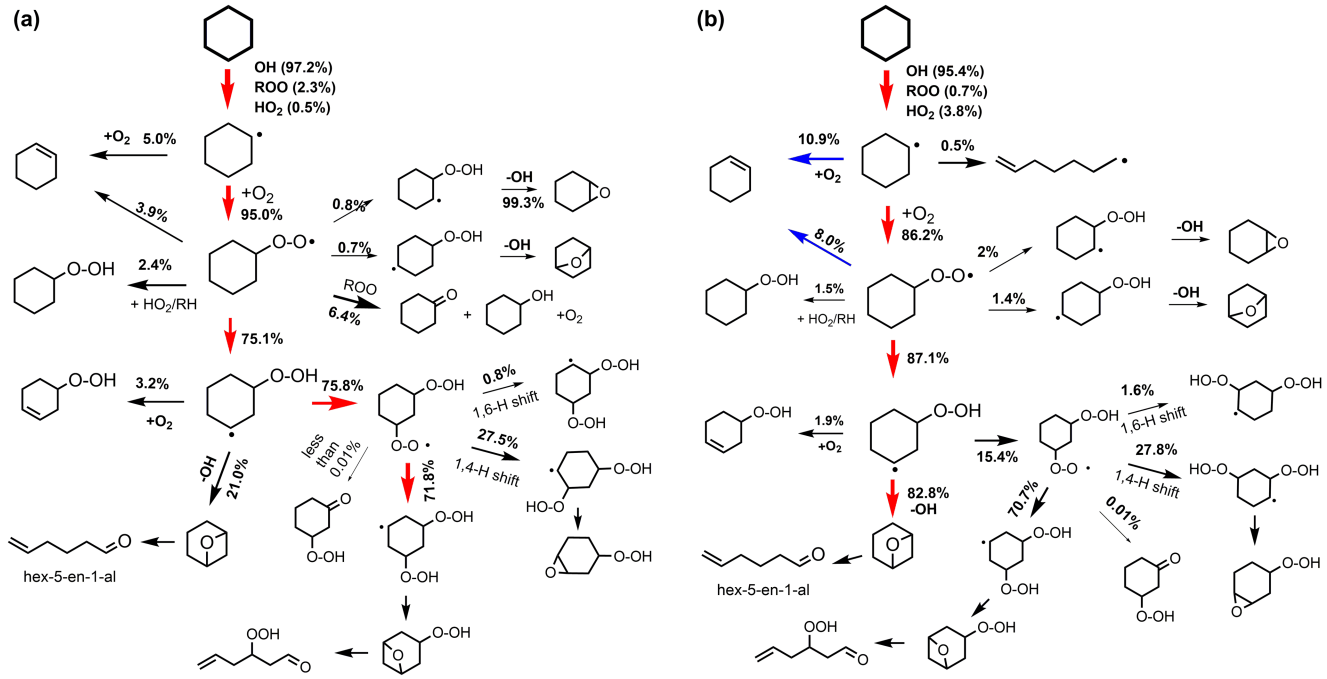

FIG. 6 Reaction networks of stoichiometric cyclohexane oxidation at (a) 575 K and (b) 660 K.

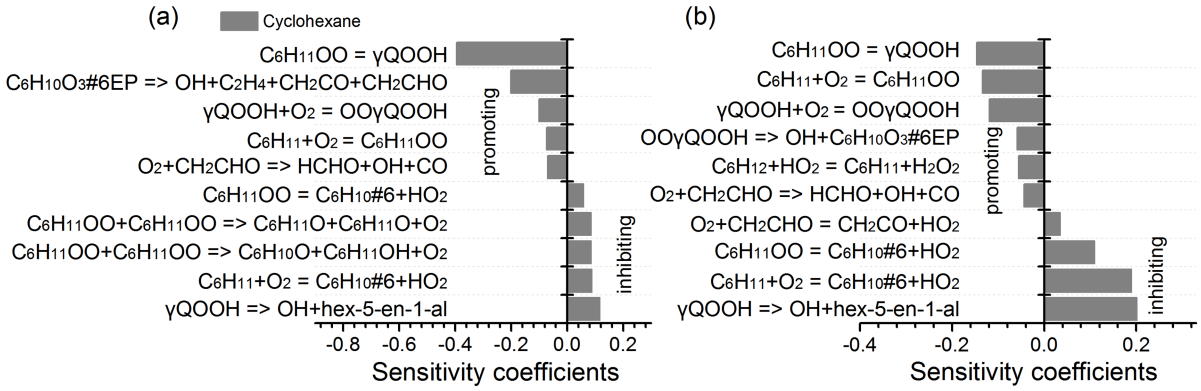

FIG. 7 Sensitivity analysis for the consumption of cyclohexane at ϕ=1.0 and (a) 575 K, (b) 660 K.

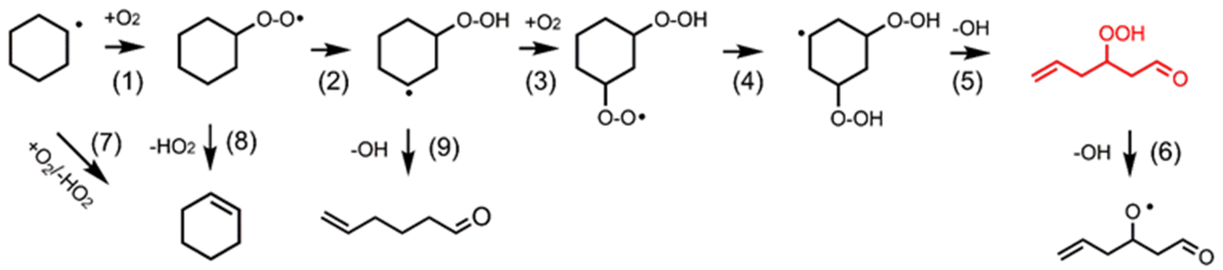

Scheme 1 Major reaction sequences from cyclohexyl radical in the low-temperature oxidation of cyclohexane.

DOI:10.1063/1674-0068/31/cjcp1806135

ity analysis in FIG. 7 shows that this reaction has a greatly enhanced positive sensitivity coefficient in the NTC region, compared with the situation in the low-temperature oxidation region.

Due to the symmetric molecular structure, the isomerization of ROO to QOOH includes four competing channels, producing αQOOH, βQOOH, γQOOH, and δQOOH (R1−R4). As shown in FIG. 1, the 1,5-H shift through a six-membered ring transition state (R3) is more favored in the isomerization of cyclohexylperoxy radical due to the reduced ring strain effect. The ROP analysis shows that the product of R3, *i.e.* γQOOH, is the dominant QOOH in the low-temperature oxidation of cyclohexane, while only trace amounts of βQOOH and δQOOH (less than 2%) are formed. For αQOOH, it is produced from the isomerization of ROO (R1) through a four-membered ring transition state with an extremely high ring strain energy. Thus R1 only has negligible contributions to the consumption of ROO. Besides the isomerization to QOOH, ROO can also be consumed by some other reactions. It can suffer the concerted elimination to produce cyclohexene and HO_2 radical (R6), the reactions with cyclohexane or HO_2 radical to produce $C_6H_{11}OOH$, and the reaction with another ROO to produce cyclohexanone and cyclohexanol. The results of cyclohexene, cyclohexyl hydroperoxide, cyclohexanone, and cyclohexanol are shown in FIGs. 4 and 5. In particular, strong competition between R3 (step (2) in Scheme 1) and R6 (step (8) in Scheme 1) can be observed from the ROP analysis and the sensitivity analysis. Same as R5, R6 is also a chain inhibition reaction. The contribution of R6 to the consumption of ROO is doubled from 575 K to 660 K and its sensitivity coefficient in FIG. 7 also greatly increases. Meanwhile the sensitivity coefficient of R3 decreases a lot.

γQOOH also has several competing consumption pathways. At 575 K, its consumption is mainly controlled by the second O_2 addition forming OOγQOOH. In order to reveal the dominant consumption pathways of OOγQOOH, quantum chemistry calculation was performed with B3LYP/6-31G(d) for optimization and CBS-QB3 for single point energy calculations. As shown in FIG. 8, the calculated results indicate the 1,5-H shift has a much lower energy barrier than other channels. Therefore the ROP analysis shows that the 1,5-H shift controls the consumption of OOγQOOH, forming $\gamma U(OOH)_2$ with the radical site on the meta position. The decomposition of $\gamma U(OOH)_2$ can produce CEHP and OH radical. The CEHP further isomerizes to KHP, while KHP suffers unimolecular decomposition to give the other OH radical and completes the chain branching process. In this work, CEHP and KHP (both are $C_6H_{10}O_3$ isomers) were observed and their results are shown in FIG. 4. The molecular structures labelled in FIG. 4 are the most possible ones proposed for $C_6H_{10}O_3$ based on the ROP analysis. Similar to R5, $\gamma Q(OOH)$ can also react with O_2 (R7−R8) to produce OFHPs

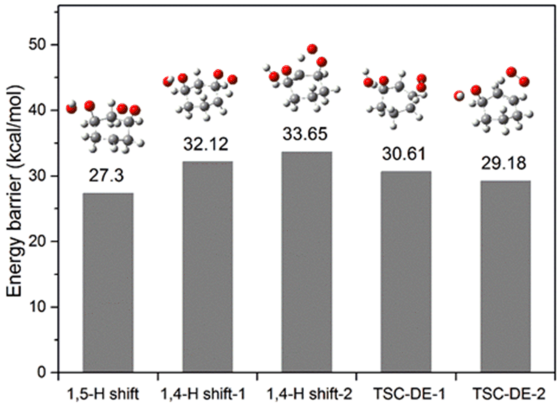

FIG. 8 Calculated energy barriers for OOQOOH isomerization channels. TSC-DE-i (i=1, 2) refers to concerted elimination in isomerization process. The optimized structures for the transition states in intermolecular H shifts are provided.

(*i.e.* C_6H_9OOH). Similar to CH_3OOH and $C_6H_{11}OOH$, the evolution of $C_6H_{10}O_3$ and C_6H_9OOH presents the same characteristics. Once generated, they decompose rapidly. The present model can well predict this tendency as well as the survived temperature region of these hydroperoxides. The survived temperature region of these hydroperoxides presented in FIG. 4 also reveals that the production and decomposition of hydroperoxides promote the fuel decomposition at initial stage (580−600 K in this work).

Besides the chain branching reaction sequence, γQOOH can also suffer the unimolecular decomposition reaction to produce 1,3-epoxycyclohexane and OH radical. However, 1,3-epoxycyclohexane is not stable and can quickly be isomerized to hex-5-en-1-al, which was first experimentally confirmed by Handford-Styring *et al.* [53] and widely incorporated in previous models [11, 18, 30]. According to the predicted results in FIG. 5, the maximum mole fraction of hex-5-en-1-al is more than one order of magnitude higher than those of cyclic ethers, aldehydes and ketones, which is similar to the GC observations of Serinyel *et al.* [18]. In both the Serinyel model and the present model, this reaction sequence was lumped as a global reaction (R9). As shown in FIG. 6, this chain propagation step is only a minor pathway to the consumption of γQOOH compared with the chain branching process at 575 K. As the temperature increases, this process becomes more and more competitive. At 660 K, it dominates the consumption of γQOOH while the chain branching process becomes less important. The sensitivity analysis also reveals the great enhancement of R9 at 660 K compared with the situation at 575 K.

According to the above discussions, both the ROP analysis and the sensitivity analysis demonstrate that the chain branching process (steps (1)−(6) in Scheme 1) can promote the low-temperature reactivity of cyclo-

DOI:10.1063/1674-0068/31/cjcp1806135

hexane. In contrast, the chain inhibition and chain propagation reactions (steps (7)−(9) in Scheme 1), including the reaction between cyclohexyl radical and O_2 forming cyclohexene and HO_2 radical (R5), the concerted elimination of ROO producing cyclohexene and HO_2 radical (R6), and the decomposition of γ-QOOH to hex-5-en-1-al and OH radical (R9), can greatly reduce the reactivity. Under the low-temperature oxidation region (580−620 K), the chain branching process dominates the oxidation, showing enhanced reactivity as the temperature increases. Then the chain inhibition and chain propagation processes become more and more competitive, leading to the reduced low-temperature reactivity and the NTC behavior over 620−660 K. The updated key reactions in the low-temperature mechanism of cyclohexane are the reason that the present model can better capture the low-temperature oxidation characteristics and NTC behavior of cyclohexane than previous models.

V. CONCLUSION

In this work, the SVUV-PIMS method was used to explore the low-temperature kinetics of cyclohexane in a jet-stirred reactor. Major products, cyclic olefins, and oxygenated product including hydroperoxides and high oxygen compounds were detected. Cyclohexane exhibits apparent low-temperature reactivity and narrow low-temperature window. A kinetic model was developed from a previous model and a series of key low-temperature reactions were updated. Compared with previous models, the present model shows satisfactory performance in capturing the experimental results. Both the ROP analysis and the sensitivity analysis were performed to help understand the chemistry in low-temperature cyclohexane oxidation. Unlike alkanes, the 1,5-H shift, instead of the 1,4- and 1,6-H shift, dominates the crucial isomerization steps of the first and second O_2 addition products in the low-temperature chain branching of cyclohexane. The NTC behavior of cyclohexane oxidation results from the reduced chain branching due to the competition between chain inhibition and propagation reactions, *i.e.* the reaction between cyclohexyl radical and O_2 and the decomposition of cyclohexylperoxy radical, both producing cyclohexene and HO_2 radical, as well as the decomposition of cyclohexylhydroperoxy radical producing hex-5-en-1-al and OH radical.

VI. ACKNOWLEDGEMENTS

The work was supported by the National Natural Science Foundation of China (No.91641205, No.51622605, No.91541201) and the Shanghai Science and Technology Committee (No.17XD1402000). The technical assistance from Mr. Yitong Zhai and Mr. Chuangchuang Cao from National Synchrotron Radiation Laboratory is deeply appreciated.

[1] R. D. Reitz, Combust. Flame **160**, 1 (2013).
[2] A. K. Agarwal, A. P. Singh, and R. K. Maurya, Prog. Energy Combust. Sci. **61**, 1 (2017).
[3] R. D. Reitz and G. Duraisamy, Prog. Energy Combust. Sci. **46**, 12 (2015).
[4] T. A. Litzinger, Prog. Energy Combust. Sci. **16**, 155 (1990).
[5] M. Mehl, T. Faravelli, E. Ranzi, T. Lucchini, A. Onorati, F. Giavazzi, P. Scorletti, and D. Terna, Kinetic Modeling of Knock Properties in Internal Combustion Engines, SAE Technical Paper, (2006).
[6] L. Shafer, R. Striebich, J. Gomach, and T. Edwards, *Chemical Class Composition of Commercial Jet Fuels and Other Specialty Kerosene Fuels*, 14th AIAA/AHI Space Planes and Hypersonic Systems and Technologies Conference, 7972 (2006).
[7] C. K. Westbrook, P. J. Smith, *Fuel Utilization, in: Basic Research Needs for Clean and Efficient Combustion of 21st Century Transportation Fuels*, A. McIlroy and G. McRae, Eds. US Department of Energy: Washington, DC (2006).
[8] W. S. Neill, W. L. Chippior, J. Cooley, M. Doma, C. Fairbridge, R. Falkiner, R. L. McCormick and K. Mitchell, *Emissions from Heavy-Duty Diesel Engine with EGR using Fuels Derived from Oil Sands and Conventional Crude*, Society of Automotive Engineers Paper No.2003-01-3144 (2003).
[9] F. L. Dryer, Proc. Combust. Inst. **35**, 117 (2015).
[10] T. Edwards, M. Colket, N. Cernansky, F. Dryer, F. Egolfopoulos, D. Friend, E. Law, D. Lenhert, P. Lindstedt, and H. Pitsch, *Development of an Experimental Database and Kinetic Models for Surrogate Jet Fuels*, 45th AIAA Aerospace Sciences Meeting and Exhibit, 770 (2007).
[11] B. Sirjean, F. Buda, H. Hakka, P. A. Glaude, R. Fournet, V. Warth, F. Battin-Leclerc, and M. Ruiz-Lopez, Proc. Combust. Inst. **31**, 277 (2007).
[12] S. M. Daley, A. M. Berkowitz, and M. A. Oehlschlaeger, Int. J. Chem. Kinet. **40**, 624 (2008) .
[13] Z. Hong, K. Y. Lam, D. F. Davidson, and R. K. Hanson, Combust. Flame **158**, 1456 (2011).
[14] Z. Tian, Y. Zhang, F. Yang, L. Pan, X. Jiang, and Z. Huang, Energy Fuels **28**, 7159 (2014).
[15] Z. M. Tian, Y. J. Zhang, F. Y. Yang, and Z. H. Huang, Energy Fuels **29**, 2685 (2015).
[16] C. S. McEnally and L. D. Pfefferle, Combust. Flame **136**, 155 (2004).
[17] W. Fujia, A. P. Kelley, and C. K. Law, Combust. Flame 159, 1417 (2012).
[18] Z. Serinyel, O. Herbinet, O. Frottier, P. Dirrenberger, V. Warth, P. A. Glaude, and F. Battin-Leclerc, Combust. Flame **160**, 2319 (2013).
[19] S. G. Davis and C. K. Law, Combust. Sci. and Tech. **140**, 427 (1998).
[20] C. S. Ji, E. Dames, B. Sirjean, H. Wang, and F. N. Egolfopoulos, Proc. Combust. Inst. **33**, 971 (2011).
[21] M. E. Law, P. R. Westmoreland, T. A. Cool, J. Wang, N. Hansen, C. A. Taatjes, and T. Kasper, Proc. Com-

DOI:10.1063/1674-0068/31/cjcp1806135

bust. Inst. **31**, 565 (2007).
[22] A. Ciajolo, A. Tregrossi, M. Mallardo, T. Faravelli, and E. Ranzi, Proc. Combust. Inst. **32**, 585 (2009).
[23] W. Li, M. E. Law, P. R. Westmoreland, T. Kasper, N. Hansen, and K. Kohse-Hoeinghaus, Combust. Flame **158**, 2077 (2011).
[24] D. Voisin, A. Marchal, M. Reuillon, J. C. Boettner, and M. Cathonnet, Combust. Sci. Tech. **138**, 137 (1998).
[25] A. El Bakli, M. Braun-Unkhoff, P. Dagaut, P. Frank, and M. Cathonnet, Proc. Combust. Inst. **28**, 1631 (2000).
[26] Z. Wang, Z. Cheng, W. Yuan, J. Cai, L. Zhang, F. Zhang, F. Qi, and J. Wang, Combust. Flame **159**, 2243 (2012).
[27] O. Lemaire, M. Ribaucour, M. Carlier, and R. Minetti, Combust. Flame **127**, 1971 (2001).
[28] S. Vranckx, C. Lee, H. K. Chakravarty, and R. X. Fernandes, Proc. Combust. Inst. **34**, 377 (2013).
[29] Y. Yang, A. L. Boehman, and J. M. Simmie, Combust. Flame **157**, 2369 (2010).
[30] F. Buda, B. Heyberger, R. Fournet, P. A. Glaude, V. Warth, and F. Battin-Leclerc, Energy Fuels **20**, 1450 (2006).
[31] B. Sirjean, P. A. Glaude, M. F. Ruiz-Lopèz, and R. Fournet, J. Phys. Chem. A **112**, 11598 (2008).
[32] B. Sirjean, P. A. Glaude, M. F. Ruiz-Lopez, and R. Fournet, J. Phys. Chem. A **113**, 6924 (2009).
[33] Z. Zhou, X. Du, J. Yang, Y. Wang, C. Li, S. Wei, L. Du, Y. Li, F. Qi, and Q. Wang, J. Synchrot. Radiat. **23**, 1035 (2016).
[34] X. Zhang, L. Ye, Y. Li, Y. Zhang, C. Cao, J. Yang, Z. Zhou, Z. Huang, and F. Qi, Combust. Flame **191**, 431 (2018).
[35] U. Struckmeier, P. Oßwald, T. Kasper, L. Böhling, M. Heusing, M. Köhler, A. Brockhinke, and K. Kohse-Höinghaus, Z. Phys. Chem. **223**, 503 (2009).
[36] P. Azay and G. Côme, Ind. Eng. Chem. Process. Des. Dev. **18**, 754 (1979).
[37] Y. Li, L. Zhang, Z. Tian, T. Yuan, J. Wang, B. Yang, and F. Qi, Energy Fuels **23**, 1473 (2009).
[38] Photoionization Cross Section Database (Version 1.0), 2011. http://flame.nsrl.ustc.edu.cn/en/database.htm.
[39] A. Rodriguez, O. Herbinet, X. Z. Meng, C. Fittschen, Z.D. Wang, L. L. Xing, and L. D. Zhang, F. Battin-Leclerc, J. Phys. Chem. A **121**, 1861 (2017).
[40] C. Cavallotti, R. Rota, T. Faravelli, and E. Ranzi, Proc. Combust. Inst. **31**, 201 (2007).
[41] E. Ranzi, M. Dente, A. Goldaniga, G. Bozzano, and T. Faravelli, Prog. Energy Combust. Sci. **27**, 99 (2001).
[42] S. Handford-Styring, R. Walker, Phys. Chem. Chem. Phys. **3**, 2043 (2001).
[43] E. J. Silke, W. J. Pitz, C. K. Westbrook, and M. Ribaucour, J. Phys. Chem. A **111**, 3761 (2007).
[44] R. X. Fernandes, J. Zador, L. E. Jusinski, J. A. Miller, C. A. Taatjes, Phys. Chem. Chem. Phys. **11**, 1320 (2009).
[45] W. J. Pitz, C. V. Naik, T. N. Mhaoldúin, C. K. Westbrook, H. J. Curran, J. P. Orme, and J. M. Simmie, Proc. Combust. Inst. **31**, 267 (2007).
[46] S. K. Gulati and R. W. Walker, J. Chem. Soc., Perkin Trans. 2 **85**, 1799 (1989).
[47] S. Granata, T. Faravelli, and E. Ranzi, Combust. Flame **132**, 533 (2003).
[48] R. J. Kee, F. M. Rupley, J. A. Miller, M. Coltrin, J. Grcar, E. Meeks, H. Moffat, A. Lutz, G. Dixon-Lewis, M. D. Smooke, *CHEMKIN-PRO 15083*, Reaction Design: San Diego (2009).
[49] F. Battin-Leclerc, O. Herbinet, P.A. Glaude, R. Fournet, Z. Zhou, L. Deng, H. Guo, M. Xie, F. Qi, Angew. Chem. **49**, 3169 (2010).
[50] Z. D. Wang, O. Herbinet, Z. J. Cheng, B. Husson, R. Fournet, F. Qi, and F. Battin-Leclerc, J. Phys. Chem. A **118**, 5573 (2014).
[51] F. Battin-Leclerc, Prog. Energy Combust. Sci. **34**, 440 (2008).
[52] J. Zádor, C. A. Taatjes, and R. X. Fernandes, Prog. Energy Combust. Sci. **37**, 371 (2011).
[53] S. M. Handford-Styring and R. W. Walker, J. Chem. Soc. Faraday Trans. **91**, 1431 (1995).

Yu-yang Li obtained his Ph.D. degree in Engineering Thermophysics in 2010 at University of Science and Technology of China. He is now an associate professor at School of Mechanical Engineering, Shanghai Jiao Tong University. His research interests are focused on combustion chemistry, flame dynamics, and multiphase processes in combustion. He has published more than 100 peer-reviewed journal papers and delivered more than 10 plenary/invited lectures. His research has been recognized by many international/domestic organizations, such as the Young Investigator Prize from the Asia Pacific Conference on Combustion (2017), the National Science Fund for Excellent Young Scholars from the National Natural Science Foundation of China (2016), the Science & Technology Award of Anhui Province (Grade 1) (2nd accomplisher, 2013) and the Bernard Lewis Fellowship from the Combustion Institute (2010).

Fei Qi obtained his Ph.D. degree in Synchrotron Radiation and its Applications in 1997 at University of Science and Technology of China. He is now a professor at School of Mechanical Engineering, Shanghai Jiao Tong University. His research interests are focused on combustion diagnostics and combustion chemistry. He has published more than 200 peer-reviewed journal papers and delivered more than 40 plenary/invited lectures. He received the National Science Fund for Outstanding Young Scholars from the National Natural Science Foundation of China (2009) and is a fellow of the Combustion Institute (2018) and the American Physics Society (2012). He is now the Secretary for Section Affairs of the Combustion Institute (2016–2020) and will be a Program Co-Chair for the 38th International Symposium on Combustion (2020).

DOI:10.1063/1674-0068/31/cjcp1806135